ARTICLES

Periodic solutions and bifurcation behavior in the parametrically damped two-well Duffing equation

Fagen Xie and Gang Hu
Center of Theoretical Physics, Chinese Center of Advanced Science and Technology (World Laboratory), Beijing, China;
Department of Physics, Beijing Normal University, Beijing 100875, China;
and Institute of Theoretical Physics, Academia Sinica, Beijing 100080, China
(Received 21 July 1994; revised manuscript received 7 December 1994)

We determine the stability boundaries of the stationary solutions of the parametrically damped two-well Duffing equation in terms of Floquet theory. The bifurcation behavior at the stability boundaries is investigated in detail. Many low primitive periodic solutions and their bifurcation structures in the parameter plane have been found by numerical simulation. The coexisting attractors of this system are also discussed.

PACS number(s): 05.45.+b

I. INTRODUCTION

For a damped nonlinear dynamical system, an external periodic force may be introduced in at least two typical ways. One is an additive form

$$\frac{d^2x}{dt^2}+k\frac{dx}{dt}+\frac{dV(x)}{dx}=F\sin\Omega t\ ; \tag{1}$$

the other is a parametric modulation form

$$\frac{d^2x}{dt^2}+k(1+F\sin\Omega t)\frac{dx}{dt}+\frac{dV(x)}{dx}=0\ , \tag{2}$$

where k, F, and Ω are the damping coefficient, the forcing amplitude, and the forcing frequency, respectively. $V(x)$ is the potential function of the system. When the potential function takes the form

$$V(x)=-\cos x\ , \tag{3}$$

Eqs. (1) and (2) become the forced damped pendulum and the parametrically damped pendulum, respectively. They all can exhibit complicated dynamical behavior, such as period-doubling bifurcation leading to chaos and transient chaos, and so on [1–3]. When the potential function is

$$V(x)=\frac{x^4}{4}-\frac{x^2}{2}\ , \tag{4}$$

Eqs. (1) and (2) become

$$\frac{d^2x}{dt^2}+k\frac{dx}{dt}+x^3-x=F\sin\Omega t\ , \tag{5}$$

$$\frac{d^2x}{dt^2}+k(1+F\sin\Omega t)\frac{dx}{dt}+x^3-x=0\ , \tag{6}$$

respectively. Equation (5) is just the well-known driven damped two-well Duffing equation. The system can exhibit rich and complicated bifurcation behavior in the parameter space [4–7]. Equation (6) is the parametrically damped two-well Duffing equation, which will be investigated in detail in this presentation. In contrast to Eq. (5), Eq. (6) always possesses one pair of stationary solutions $x=\pm1$, $\dot{x}=0$, which, however, may be unstable against certain perturbations. The stability boundaries of these solutions can be discussed by using the methods of Lindstedt-Poincaré perturbation and Floquet theory [2,3]. In this paper we mainly study the dynamical behavior of the parametrically damped two-well Duffing equation.

This paper is organized as follows. In the next section we discuss the symmetry of the two classes of dissipative differential equations. In Sec. III we determine the stability boundaries of the pair of stationary solutions using the Floquet theorem. In Sec. IV we investigate the bifurcation behavior at the stability boundaries numerically. In Sec. V we study the bifurcation behavior of some low periodic solutions in the parameter plane and the basin structure of a number of coexisting attractors. Finally, in Sec. VI we make a few concluding remarks.

II. THE DISCRETE SYMMETRY OF TWO CLASSES OF DISSIPATIVE DIFFERENTIAL EQUATIONS

Denoting $y=dx/dt$, Eqs. (1) and (2) can be rewritten as

$$\begin{aligned}\frac{dx}{dt}&=y\ ,\\ \frac{dy}{dt}&=-ky-\frac{dV(x)}{dx}+F\sin\Omega t;\end{aligned} \tag{7}$$

$$\begin{aligned}\frac{dx}{dt}&=y\ ,\\ \frac{dy}{dt}&=-k(1+F\sin\Omega t)y-\frac{dV(x)}{dx}\ ,\end{aligned} \tag{8}$$

respectively. If $V(-x)=V(x)$ we can introduce two

transformations T_1 and T_2 for Eqs. (7) and (8)

$$T_1(x,y,t)=\left[-x,-y,t+\frac{\pi}{\Omega}\right], \tag{9}$$

$$T_2(x,y,t)=\left[-x,-y,t+\frac{2\pi}{\Omega}\right], \tag{10}$$

respectively. If $X=(x(t),y(t))$ is a solution of Eq. (7) [(8)], then T_1X [T_2X] is also a solution of the respective equations. The difference between the two transformations is that the time shift of Eq. (9) is a half period of the driven force, but that of Eq. (10) is a whole period of the force. Transformation T_1 generates an antisymmetry of Eq. (7) between any two Poincaré sections with a phase difference of a half period π/Ω and T_2 generates an antisymmetry of Eq. (8) with, however, a phase shift of a whole period of the external force. Using periodicity of the external force, we have

$$T_{1,2}^2=1 . \tag{11}$$

$T_{1,2}$ divide the orbits of Eqs. (7) and (8) into two classes in accordance with the eigenvalues of $T_{1,2}$. If $T_{1,2}X=X$, X is symmetric; if $T_{1,2}X=-X$, it is asymmetric. In general, for a symmetric orbit, its eigenvalues are positive. Therefore, the symmetry must be broken before the period-doubling bifurcation, where the relevant eigenvalue is -1.

III. STABILITY BOUNDARIES OF THE STATIONARY SOLUTIONS

For convenience we rewrite Eq. (6) as

$$\omega^2\frac{d^2x}{dt}+q[1+2\epsilon\sin(2t)]\frac{dx}{dt}+x^3-x=0 , \tag{12}$$

where we use rescalings

$$t\to\frac{2t}{\Omega},\quad \omega=\frac{\Omega}{2},\quad q=\frac{k\omega}{2},\quad \epsilon=\frac{F}{2} . \tag{13}$$

The linearized equation for a perturbation ξ around the pair of stationary solutions $x=\pm1$, $\dot{x}=0$, reads

$$\omega^2\ddot{\xi}+q(1+2\epsilon\sin2t)\dot{\xi}+2\xi=0 . \tag{14}$$

The stability boundaries of the stationary solutions of Eq. (12) can be determined from this linearized equation. According to the Floquet theorem, a Floquet multiplier must vanish at the stability boundaries. Thus we may assume the existence of

$$\xi=A_0+\sum_{n=1}^{\infty}(A_n\cos nt+B_n\sin nt) . \tag{15}$$

Inserting expression (15) into Eq. (14) and comparing each harmonics on both sides of the equation, we obtain

$$\begin{aligned}&(2-n^2\omega^2)A_n+nqB_n\\&\qquad+q\epsilon[(n-2)A_{n-2}-(n+2)A_{n+2}]=0 ,\\&(2-n^2\omega^2)B_n-nqA_n\\&\qquad+q\epsilon[(n-2)B_{n-2}-(n+2)B_{n+2}]=0 ,\end{aligned} \tag{16}$$

where we have used the identities $A_{-n}=A_n$ and $B_{-n}=-B_n$. It is obvious that the solutions of Eq. (16) decompose into two independent classes, one involving odd n and another even n. No nontrivial solution exists for the latter, so we need to consider only odd n. For the lowest-order approximation we can truncate Eq. (16) at $n=1$ and obtain the two equations

$$\begin{aligned}&(2-\omega^2-q\epsilon)A_1+qB_1=0 ,\\&(2-\omega^2+q\epsilon)B_1-qA_1=0 .\end{aligned} \tag{17}$$

The existence of a nontrivial solution requires the determinant of the coefficient matrix to vanish

$$\begin{vmatrix}2-\omega^2-q\epsilon & q\\ -q & 2-\omega^2+q\epsilon\end{vmatrix}=0 , \tag{18}$$

which gives rise to

$$\epsilon_c^{(1)}=q^{-1}\sqrt{(2-\omega^2)^2+q^2} . \tag{19}$$

The next approximation is obtained from the truncation at $n=3$. From Eq. (16) four equations for A_1, A_3, B_1, and B_3, similar to Eq. (17), may be derived and the condition for the existence of a nontrivial solution becomes

$$\begin{vmatrix}2-\omega^2-q\epsilon & q & -3q\epsilon & 0\\ -q & 2-\omega^2+q\epsilon & 0 & -3q\epsilon\\ q\epsilon & 0 & 2-9\omega^2 & 3q\\ 0 & q\epsilon & -3q & 2-9\omega^2\end{vmatrix}=0 . \tag{20}$$

From Eq. (16) any finite higher-order approximations of the critical condition may be found. We show a result which is obtained at the truncation $n=5$ in Fig. 1 by the dashed lines. The threshold is very close to the solid lines

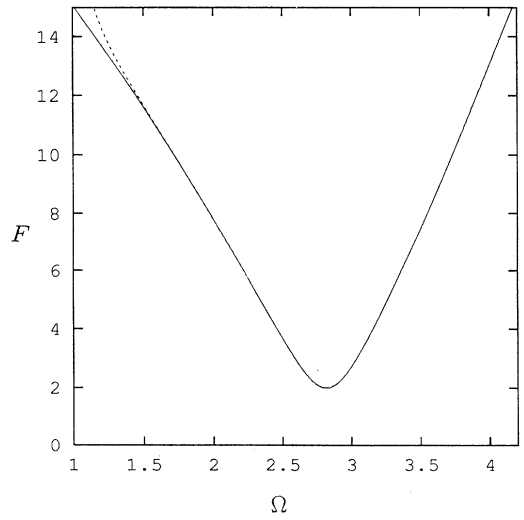

FIG. 1. Stability boundary of the stationary solutions $x=\pm1$, $\dot{x}=0$ in the Ω-F parameter plane. $k=0.2$ for this figure and all the following figures. The solid lines are determined by the exact computation (one eigenvalue of the pair of stationary solutions is equal to -1). The dashed lines are obtained in terms of the Floquet theorem at the truncation $n=5$.

determined by the exact computation. The parameter k is fixed at 0.2 throughout the paper.

IV. BIFURCATION BEHAVIOR AT THE STABILITY BOUNDARIES

The stability boundary of the solutions $x=\pm 1$, $\dot{x}=0$ is V shaped as shown in Fig. 1. At this stability boundary, a common feature is that one of the eigenvalues of the stationary solutions is always -1. However, the bifurcation behavior is rather rich along the boundary, i.e., the dynamics is rather different and interesting as the parameters are varied to cross different segments of this boundary. On the right-hand segment of the V-shaped curve there is period-doubling bifurcation. We show a bifurcation diagram in Fig. 2(a) along the vertical line $\Omega=3.3$, where x is plotted at $t=2\pi n$ with n being large enough to completely exclude the transient process. The numerical result shows that a period-two solution arises via period-doubling bifurcation at $F=5.385$, right at the critical value theoretically predicted in Fig. 1. From the figure it is clear that a symmetric period-two orbit coexists with this period-doubling asymmetric orbit and both attractors form an interesting hysteresis phenomenon.

On the left-hand segment of the stability boundary of Fig. 1, the critical eigenvalue of the stationary solutions is still equal to -1; however, the bifurcation behavior is completely different and much more complicated. As $\Omega>2.49$, when the stationary solutions lose their stability, the system can be attracted to another single-well (asymmetric) attractor, which may be periodic (with periods two, four, eight, etc.) or chaotic, according to the values of Ω. From Figs. 2(b)–2(d) we fix different Ω and increase F to cross the left-hand side of the V-shaped curve of Fig. 1. The variety of the bifurcations on a single critical curve show the rather rich dynamic behavior of our model. In each figure the $x=1$, $\dot{x}=0$ stationary solution loses its stability, via saddle-node bifurcation, at the critical F value predicted in Fig. 1 with very high precision. As Ω decreases the asymptotic state of the system, after the instability of the steady solution, changes from periodic orbit to small region chaos and then to large region chaos, as shown in Figs. 2(b)–2(d).

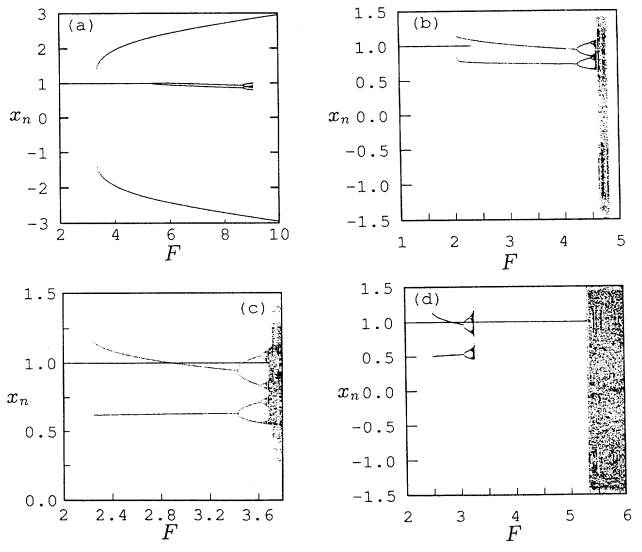

FIG. 2. Plots of x at $t=2\pi n$, with n being large enough to exclude the transient process, versus F. (a) $\Omega=3.3$, (b) $\Omega=2.7$, (c) $\Omega=2.495$, and (d) $\Omega=2.3$.

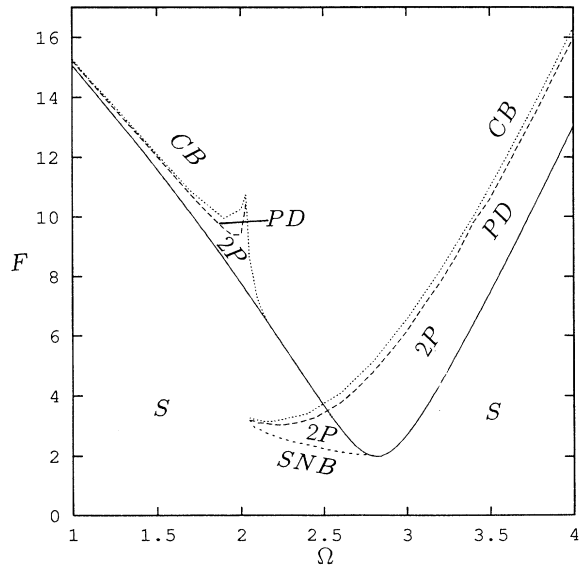

FIG. 3. The solid line indicates the stability boundary of the stationary solutions. The notations SNB, PD, and CB represent the saddle-node bifurcation curve, the period-doubling bifurcation curve, and the boundary of the chaotic region, respectively. nP denotes the period-n motion.

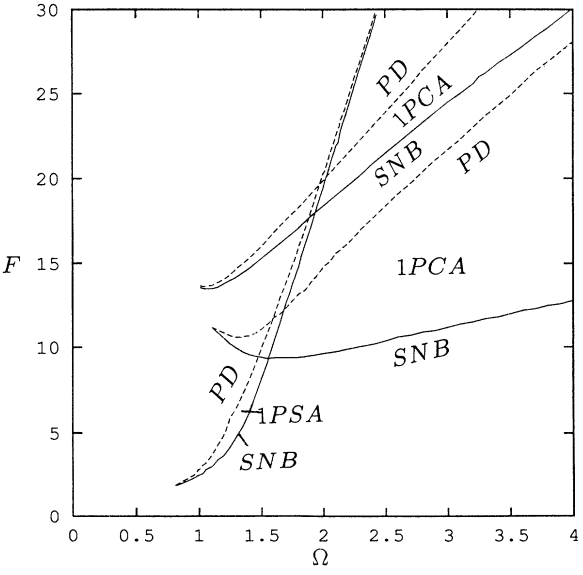

FIG. 4. Bifurcation structure of 1P asymmetric solutions in the Ω-F plane. 1PSA and 1PCA denote period-one asymmetric single-well and cross-well motions, respectively. All other notations have the same meaning as in Fig. 3.

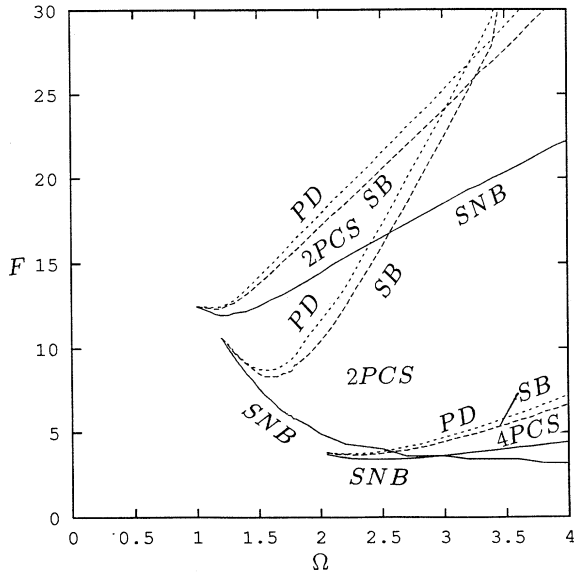

FIG. 5. Bifurcation structure of the symmetric 2P and 4P solutions in the Ω-F plane. 2PCS and 4PCS denote symmetric cross-well period-two and -four motions, respectively. SB represents the symmetry-breaking bifurcation curve. All other notations have the same meaning as in Fig. 3.

It is interesting to remark that as $2.1 \leq \Omega \leq 2.49$, the motion of the system after instability turns out to be large-scale cross-well chaos via an intermittency; at the critical point one eigenvalue of the stationary solutions is still -1. This is type-III intermittency according to Ref. [11]. However, as $\Omega \leq 2.1$, the behavior of the system becomes period-doubling bifurcation after the stationary solutions lose their stability.

The complicated bifurcation diagram in Fig. 2 can be much better understood in Fig. 3, where regions S, nP, PD, SNB, and CB denote the stationary solution, the period-n solution, the period-doubling bifurcation curve, the saddle-node bifurcation curve, and the boundary of the chaotic region, respectively. It is clear that through the right-hand side of the V-shaped solid curve the bifurcation is period doubled (supercritical bifurcation), through the lower part of the left wing the bifurcation is of saddle-node type (subcritical bifurcation), and the asymptotic solutions after the instability of the stationary solutions depend on where the critical boundary is crossed. Through the upper part of the left wing of the V-shaped curve, the bifurcation is again period doubled.

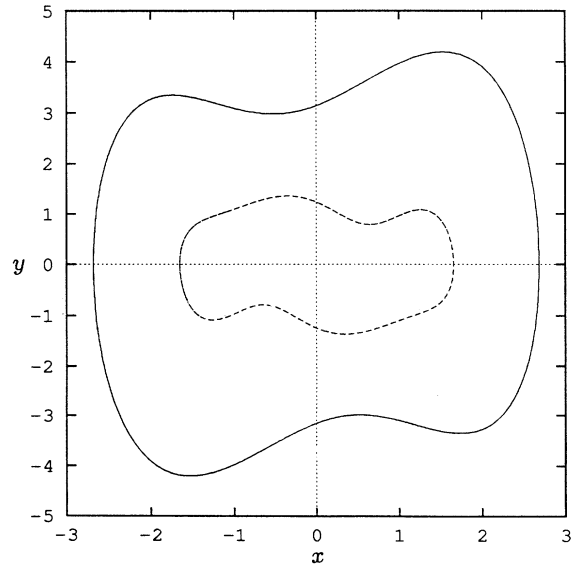

FIG. 6. Asymptotic orbits of Eq. (6) at $\Omega=3.5$, $F=5.0$. Solid line, the symmetric period-two solution; dashed line, the symmetric period-four solution.

V. COEXISTING ATTRACTORS AND THEIR BASIN BOUNDARIES

In the foregoing sections we investigated the bifurcation behavior of the system at the stability boundary of

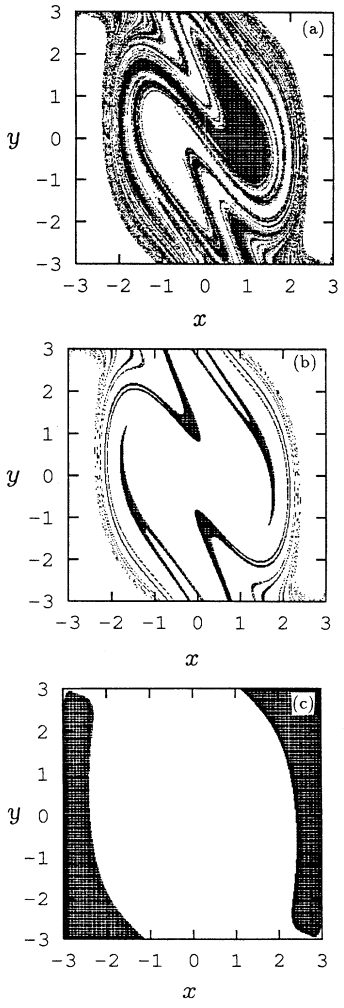

FIG. 7. Basin structure of the attractors in the Poincaré section at $\Omega=3.5$, $F=5.0$. The corresponding basins are represented by the black regions. (a) The basin of the stationary solution $x=1$, $\dot{x}=0$. The basin of the state $x=-1$. $\dot{x}=0$ can be obtained from (a) by the inversions $x,\dot{x}\rightarrow -x,-\dot{x}$. (b) The basin of the symmetric period-four solution. (c) The basin of the symmetric period-two solution.

the pair of stationary solutions. Actually, the system may have many asymptotic solutions coexisting in various parameter regions. It is very interesting to investigate the distribution of these attractors in the parameter space and their basin structure in the variable space.

First we found numerically that there are three pairs of different period-one solutions in the $\Omega - F$ plane (see Fig. 4). One pair is the single-well attractors (1PSA), the others are cross-well attractors (1PCA). They are all asymmetric (the letter S, C, and A in 1PSA and 1PCA indicate single-well, cross-well, and asymmetric, respectively). They appear via saddle-node bifurcation (solid lines) and become unstable via period-doubling bifurcation (dashed lines).

Apart from the asymmetric 2P solutions, arising via the period doubling of the period-one solutions, we also find that there are two different symmetric period-two orbits, which are all cross-well orbits (2PCS, where the letter S indicates symmetric) and shown in Fig. 5. The notation SB represents the symmetry-breaking curve. Furthermore, we also find a symmetric period-four solution (4PCS) in the parameter plane, shown in the right-lower part of Fig. 5.

If we compare Figs. 3–5, it is clear that the regions of various types of motions heavily overlap each other, indicating the coexistence of multiple attractors. In the overlapped regions, at one parameter point, the system can be attracted to different orbits, depending on the initial preparations. Then an investigation of the basin structure in the variable space turns out to be extremely interesting. As working examples, we demonstrate two cases of coexisting attractors. First, we choose the parameters $\Omega = 3.5$ and $F = 5.0$, which are located in the region where a pair of stationary solutions, a symmetric period-two solution and a symmetric period-four solution, coexist (see Figs. 3–5). We show the trajectories of the symmetric period-two and -four solutions in Fig. 6. Their corresponding basins in the Poincaré section are shown in Fig. 7. It is noticeable that the basin boundaries of the solutions tangle together and form a complicated structure in the Poincaré section. Figure 7 is made as follows. We divide the square variable region $[-3,3]\times[-3,3]$ in the Poincaré section into 300×300 grids. Then we integrate Eq. (6) exhaustively for every point on the grids, until an asymptotic state is reached; then the initial point belongs to the basin of the finally reached orbit.

At the parameters $\Omega = 1.45$ and $F = 8.5$, there are five attractors coexisting. In addition to the pair of stationary solutions, there exists a pair of single-well period-one solutions and a symmetric period-two solution (see Fig. 8). The basins of these coexisting attractors are shown in Fig. 9. The boundaries of the basins shown in Figs. 7 and 9 clearly form fractals. A similar fractal structure has

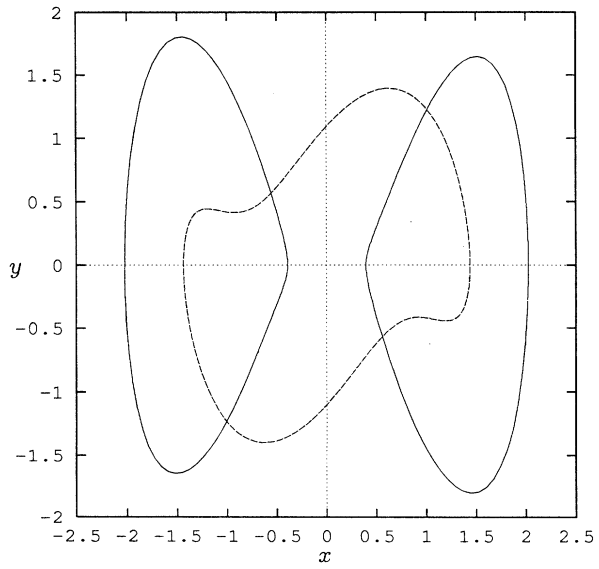

FIG. 8. Asymptotic orbits of Eq. (6) at $\Omega = 1.45$, $F = 8.5$. Solid lines, the pair of period-one solutions; dashed line, the symmetric period-two solution.

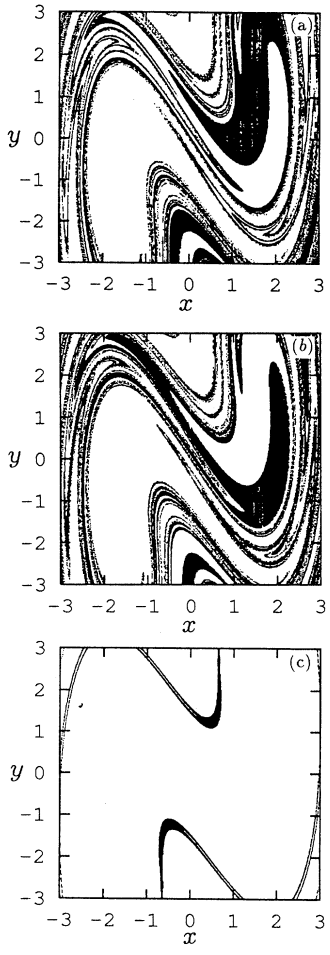

FIG. 9. Basin structure of the attractors in the Poincaré section at $\Omega = 1.45$, $F = 8.5$. The basins are still represented by the black regions. (a) The basin of the stationary solution $x = 1$, $\dot{x} = 0$. (b) The basin of the right-well period-one solution. (c) The basin of the symmetric period-two solution. The basins of $x = -1$, $\dot{x} = 0$ and the left-well 1P solution can be obtained from (a) and (b), respectively, by the inversions $x, \dot{x} \rightarrow -x, -\dot{x}$.

been reported for Eq. (5) [12]. With Eq. (6) the fractal structures are even more complicated with more basins coexisting. Since the bifurcation curves of different solutions often cross each other, the status of coexisting attractors occurs very frequently. By varying parameters, the coexisting attractors may be changed and some can be suddenly ceased by some mechanism such as the boundary crisis or fold bifurcation; here we do not discuss the details of this matter [8–10].

VI. CONCLUDING REMARKS

We have studied the dynamics of the parametrically damped two-well Duffing equation in the $\Omega-F$ plane. The following results are worth noting.

(i) The parametrically damped two-well Duffing equation always possesses a pair of stationary solutions $x=\pm 1$, $\dot{x}=0$. The stability boundary of these stationary solutions can be obtained in terms of Floquet theory. The theoretical predictions perfectly fit numerically results.

(ii) On the instability boundary with eigenvalue -1 we have found different bifurcations (both supercritical and subcritical), such as period-doubling bifurcation and saddle-node bifurcation, among others, leading to very rich destinations. The attractor distribution underlying this richness is emphasized.

(iii) Many low periodic symmetric and asymmetric orbits have been found in the parameter plane. The distribution of coexisting attractors in the parameter plane is shown numerically. We also study the basin structure of the coexisting attractors for two parameter points. An interesting fractal structure of the basin boundaries is revealed.

ACKNOWLEDGMENTS

This work was supported partially by the Chinese Natural Science Foundation and the Open Laboratories Project of Academia Sinica. Sun Microsystems, Inc. donated a workstation and Wolfram Research, Inc. donated the MATHEMATICA software to the Nonlinear Dynamics Group at ITP.

[1] J. A. Blackburn and H. J. T. Smith, Phys. Rev. A **45**, 593 (1992).
[2] Binruo Wu and J. A. Blackburn, Phys. Rev. A **45**, 7030 (1992).
[3] FaGen Xie and WeiMou Zheng, Phys. Rev. E **49**, 1888 (1994).
[4] S. Sato, M. Sano, and Y. Sawada, Phys. Rev. A **28**, 1664 (1983).
[5] Hu Gang and Bai-lin Hao, Phys. Rev. A **42**, 3335 (1990).
[6] Yoshisuke Ueda, Chaos, Solitons Fractals **1**, 199 (1991).
[7] H. G. Solari and R. Gilmore, Phys. Rev. A **38**, 1566 (1988).
[8] C. Grebogi, E. Ott, and J. A. Yorke, Phys. Rev. Lett. **48**, 1507 (1982).
[9] C. Grebogi, E. Ott, and J. A. Yorke, Phys. Rev. Lett. **57**, 1284 (1982).
[10] H. B. Stewart, J. M. T. Thompson, A. N. Lansbury, and Y. Ueda, Int. J. Bif. Chaos **1**, 265 (1991).
[11] Y. Pomeau and P. Manneville, Commun. Math. Phys. **74**, 189 (1980).
[12] C. Pezeshki and E. H. Dowell, Physica D **32**, 194 (1988).